Structure
Article

The Alternatively Spliced Acid Box Region Plays a Key Role in FGF Receptor Autoinhibition

Juliya Kalinina,[1,4,5] Kaushik Dutta,[2,5] Dariush Ilghari,[1,5] Andrew Beenken,[1] Regina Goetz,[1] Anna V. Eliseenkova,[1] David Cowburn,[2,3] and Moosa Mohammadi[1,*]
[1]Department of Pharmacology, New York University School of Medicine, 550, First Avenue, New York, NY 10016, USA
[2]New York Structural Biology Center, 89 Convent Avenue, New York, NY 10027-7566, USA
[3]Present address: Department of Biochemistry, Albert Einstein College of Medicine of Yeshiva University, 1300 Morris Park Avenue, New York, NY 10461, USA
[4]Present address: Departments of Neurosurgery, Hematology and Medical Oncology, School of Medicine, and Winship Cancer Institute, Emory University, 1365-C Clifton Road NE, Atlanta, GA 30322, USA
[5]These authors contributed equally to this work.
*Correspondence: Moosa.Mohammadi@nyumc.org
DOI 10.1016/j.str.2011.10.022

SUMMARY

Uncontrolled fibroblast growth factor (FGF) signaling can lead to human malignancies necessitating multiple layers of self-regulatory control mechanisms. Fibroblast growth factor receptor (FGFR) autoinhibition mediated by the alternatively spliced immunoglobulin (Ig) domain 1 (D1) and the acid box (AB)-containing linker between D1 and Ig domain 2 (D2) serves as the first line of defense to minimize inadvertent FGF signaling. In this report, nuclear magnetic resonance and surface plasmon resonance spectroscopy are used to demonstrate that the AB subregion of FGFR electrostatically engages the heparan sulfate (HS)-binding site on the D2 domain in *cis* to directly suppress HS-binding affinity of FGFR. Furthermore, the *cis* electrostatic interaction sterically autoinhibits ligand-binding affinity of FGFR because of the close proximity of HS-binding and primary ligand-binding sites on the D2 domain. These data, together with the strong amino acid sequence conservation of the AB subregion among FGFR orthologs, highlight the universal role of the AB subregion in FGFR autoinhibition.

INTRODUCTION

The mammalian fibroblast growth factors (FGFs) comprise a family of 18 ligands that signal through four FGF receptor tyrosine kinases (FGFR1–4) and their alternatively spliced isoforms (Johnson and Williams, 1993) to regulate embryonic development and adult metabolism (Beenken and Mohammadi, 2009; Goldfarb, 2005; Itoh and Ornitz, 2011; Kuro-o, 2008). Fibroblast growth factors adopt a β-trefoil fold consisting of 12 antiparallel β strands (β1–β12) (Faham et al., 1998; Mohammadi et al., 2005b). The heparan sulfate (HS)-binding site (HBS) of FGFs comprises residues from the β1-β2 loop and the β10-β12 region (Goetz et al., 2007).

The extracellular region of a prototypical FGFR consists of three immunoglobulin (Ig)-like domains (D1, D2, and D3) connected by flexible linkers (Plotnikov et al., 1999). A unique characteristic of FGFRs is a stretch of glutamate-, aspartate-, and serine-rich sequence situated in the D1-D2 linker, termed the acid box (AB; Johnson and Williams, 1993; Figures 1C and 1D). The segment spanning D2 and D3 (referred to as D2-D3 region) is necessary and sufficient for ligand binding and specificity (Mohammadi et al., 2005b). The HBS of FGFR is comprised of basic amino acids from the g-helix A, β strands B and D, and the gA-βA′ and βA′-βB loops—all of which localize onto one face of D2 (Schlessinger et al., 2000; Figure 1B).

HS promotes 1:1 FGF-FGFR binding and stabilizes formation of a 2:2 FGF-FGFR signal transducing dimer (Schlessinger et al., 2000) in which receptor and ligand from one 1:1 FGF-FGFR protomer interacts with the receptor from the other 1:1 FGF-FGFR protomer (Figure 1A). Heparan sulfate interacts concomitantly with the juxtaposed HBS of the FGFR D2 domains and of the FGF ligands to enhance protein-protein contacts at the dimer interface, thereby sustaining dimerization (Mohammadi et al., 2005a; Figure 1A). Dimerization enables tyrosine transphosphorylation of the intracellular kinase domains, which upregulates kinase activity (Chen et al., 2008; Mohammadi et al., 1996) and generates docking sites for recruitment and phosphorylation of downstream signaling substrates, ultimately culminating in gene expression changes and biological responses (Eswarakumar et al., 2005).

Tissue-specific alternative splicing of the D3 domain of FGFR1-3 gives rise to epithelial "b" and mesenchymal "c" isoforms of these FGFRs (Jin et al., 2004; Orr-Urtreger et al., 1993; Xu et al., 1998). This splicing event controls ligand-binding specificity of FGFRs by altering the primary sequences of key ligand-binding regions in the C-terminal half of D3 (Mohammadi et al., 2005b; Olsen et al., 2006; Yeh et al., 2003; Figure 1C). Skipping of exons encoding D1 and/or the AB-containing linker between D1 and D2 (abbreviated as AB/linker in the following text) generates isoforms lacking D1 (FGFR1c, FGFR1b, and FGFR2c), AB/linker (FGFR3c), or both D1 and AB/linker (FGFR2b; Hou et al., 1992; Shimizu et al., 2001; Xu et al., 1992). Loss of D1 or AB/linker enhances the affinity of FGFR for FGF and HS and increases the signaling capacity of FGFR, demonstrating that this alternative

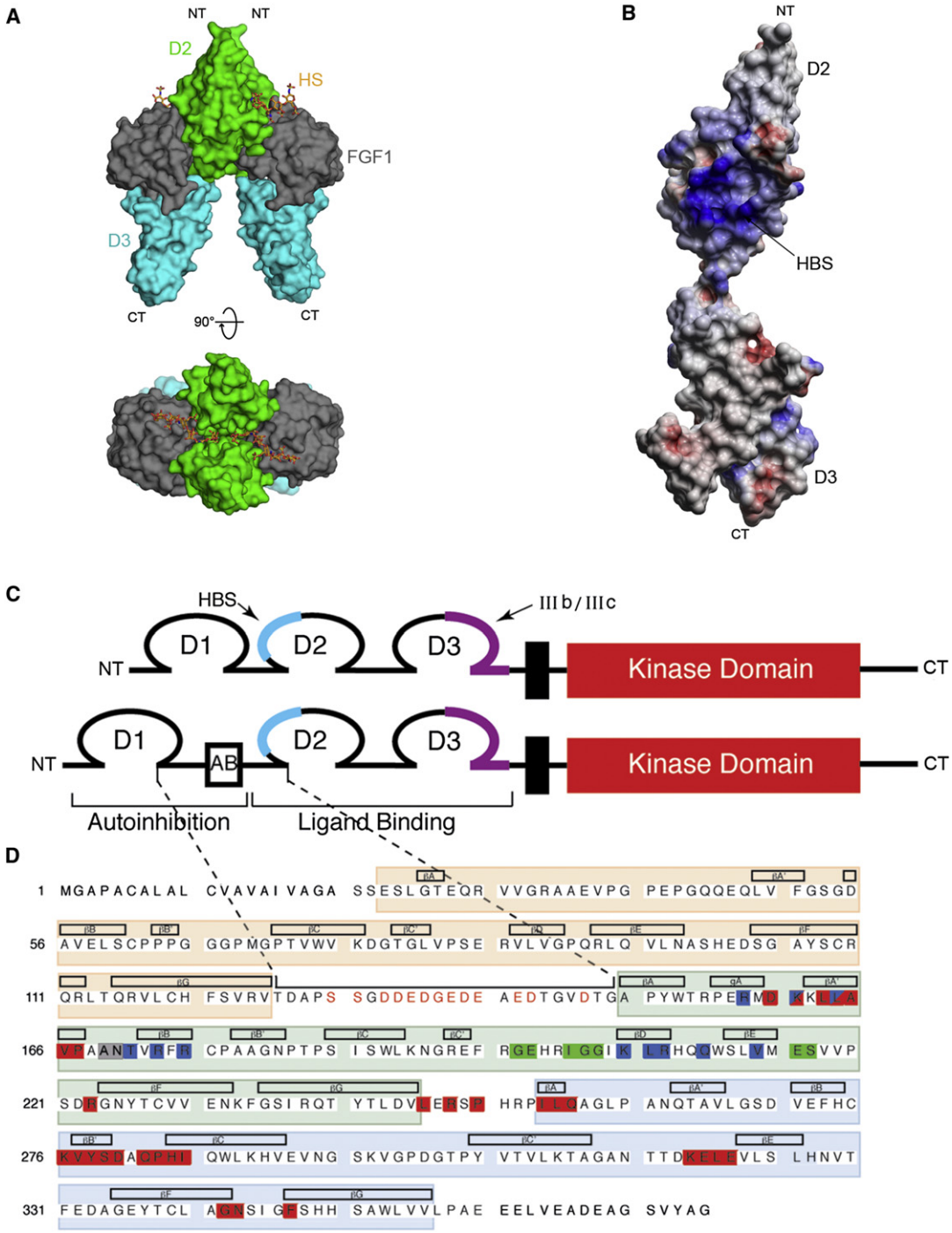

Figure 1. FGF, FGFR, and HS Form a Symmetric 2:2:2 Dimer and Alternative Splicing of the AB/linker Region of FGFR Autoinhibits FGFR Activation and Signaling

(A) Surface representation of the 2:2:2 FGF2-FGFR1c-heparin complex structure (PDB ID 1FQ9; Schlessinger et al., 2000). The molecular surfaces of D2, D3, and FGF are colored green, blue, and gray, respectively. Heparin oligosaccharides are shown as sticks.

(B) The surface charge distribution of the D2-D3 region of FGFR1c is shown (PDB ID 1FQ9; Schlessinger et al., 2000). Blue, red, and white represent the positively charged, negatively charged, and neutral regions, respectively.

(C) Schematic representation of the two alternatively spliced FGFR3c isoforms with and without the AB/linker region. The AB subregion within the AB/linker is indicated by a black box. The dashed lines show the boundaries of the exon encoding the 23-residue long AB/linker region in panel D. The HBS of the receptor is confined to D2 and is highlighted in cyan. Two alternatively spliced exons (IIIb and IIIc) code for the C-terminal half of D3.

(D) Amino acid sequence of the FGFR3c extracellular domain. Secondary structure elements are indicated atop of the sequence. Secondary structures for D2 and D3 are based on the crystal structure of FGF1-FGFR3c (PDB ID 1RY7; Olsen et al., 2004) and for D1 are based on the solution structure of FGFR1c D1 (PDB ID

splicing event controls receptor autoinhibition (Olsen et al., 2004; Roghani and Moscatelli, 2007; Shi et al., 1993; Shimizu et al., 2001; Wang et al., 1995; Xu et al., 1992). Consistent with the autoinhibitory role of D1 and AB/linker in receptor regulation, loss of these regions has been implicated in cancer (Kobrin et al., 1993; Mansson et al., 1989; Onwuazor et al., 2003; Tomlinson and Knowles, 2010; Yamaguchi et al., 1994).

The molecular mechanism by which D1 and AB/linker impose receptor autoinhibition is controversial. McKeehan and colleagues (Wang et al., 1995) proposed that the AB/linker serves merely as a "passive" flexible hinge enabling D1 to intramolecularly engage ligand- and HS-binding sites on the D2-D3 region to suppress both ligand- and HS-binding affinity of the receptor (Wang et al., 1995). Calculation of the surface electrostatic potential of the first FGF-FGFR complex structure solved in our laboratory showed that the HBS on D2 forms a contiguous positively charged surface (Plotnikov et al., 1999; Figure 1B). Based on this observation, we proposed that the negatively charged AB subregion of the AB/linker electrostatically engages the positively charged HBS of D2 to suppress HS binding. We further speculated that the electrostatic interactions of AB with D2 may in turn encourage intramolecular interactions of D1 with ligand-binding sites in the D2-D3 region to suppress ligand binding (Olsen et al., 2004). Hence, in stark contrast to the model proposed by McKeehan and colleagues (Wang et al., 1995), in our model the AB/linker region plays an active role in FGFR autoinhibition.

In this study, we explored the role of the AB/linker in FGFR autoinhibition in *cis* by nuclear magnetic resonance (NMR) and surface plasmon resonance (SPR) spectroscopy. Our data show that the AB subregion of the AB/linker electrostatically engages the HS-binding site on the D2 domain in *cis,* thereby directly suppressing HS-binding affinity of the receptor. The *cis* AB:HBS interaction also sterically autoinhibits ligand binding to the receptor because of the close proximity of the HBS and the ligand-binding site on the D2 domain. Hence, our data reveal that the AB subregion plays a key role in FGFR autoinhibition.

RESULTS

AB/Linker-Imposed Receptor Autoinhibition Is an Intrinsic Property of the Isolated FGFR3c Ectodomain

Alternative splicing of FGFR3c gives rise to two isoforms in vivo that differ only in the presence of the AB/linker region (Figures 1C and 1D; Shimizu et al., 2001). Cell-based studies have previously established that, compared to the isoform containing the AB/linker, the isoform lacking this region requires 3- to 4-fold lower concentration of HS to elicit the same level of proliferation in BaF3 cells (Shimizu et al., 2001). Moreover, at any given HS concentration, the mitogenic response of BaF3 cells expressing the isoform without the AB/linker to FGF8 and FGF9 is about 2-fold greater than that of the cells expressing the full-length receptor (Shimizu et al., 2001). Therefore, FGFR3c is an optimal FGFR for structural characterization of the role of the AB/linker in FGFR autoinhibition.

We have previously shown that an FGFR3c ectodomain fragment lacking D1 and the AB/linker region binds FGF1 and heparin with higher affinities than the full-length FGFR3c ectodomain (D1-AB-D2-D3) does (Olsen et al., 2004), demonstrating that the presence of D1 and AB/linker autoinhibits FGFR3c. Since an FGFR3c isoform lacking both D1 and the AB/linker does not occur naturally, we decided to compare heparin/HS- and ligand-binding affinities of D1-AB-D2-D3 with those of the D1-D2-D3$^{\Delta AB/linker}$ ectodomain, which represents the naturally occurring isoform of FGFR3c lacking the AB/linker. The ectodomain constructs were expressed in *Escherichia coli* (*E. coli*; Table S1 available online) and refolded from bacterial inclusion bodies and purified to homogeneity using heparin affinity and size-exclusion chromatographies (Figure S1). SPR spectroscopy was then used to compare FGF and HS binding affinities of the two ectodomains (Figure 2). For HS binding analysis, heparin was coupled to a biosensor chip and increasing concentrations of D1-AB-D2-D3 or D1-D2-D3$^{\Delta AB/linker}$ were passed over the chip (Figures 2A and 2B). For ligand binding analysis, two well-known cognate ligands of FGFR3c, namely, FGF1 and FGF8b, were immobilized on biosensor chips, and increasing concentrations of either of the two receptor ectodomains were flowed over the chips (Figures 2C–2F). D1-D2-D3$^{\Delta AB/linker}$ bound heparin with almost 3-fold higher affinity than D1-AB-D2-D3 (Table 1; Figures 2A and 2B). D1-D2-D3$^{\Delta AB/linker}$ also bound the FGF ligands with about 2-fold greater affinity than D1-AB-D2-D3 (compare Figures 2C and 2E with Figures 2D and 2F, respectively). To our knowledge, these data show for the first time that the AB/linker-imposed receptor autoinhibition occurs in the context of the isolated FGFR3c ectodomain, i.e., in the absence of transmembrane and cytoplasmic regions of receptor or any accessory "extrinsic" cellular proteins/factors. Our SPR data are consistent with the published cell-based data (Shimizu et al., 2001), demonstrating that the presence of the AB/linker region autoinhibits FGFR3c signaling by suppressing the receptor's affinity for FGF and HS.

Having confirmed the existence of AB/linker-mediated FGFR3c autoinhibition in the context of the isolated receptor ectodomain, we then expressed and purified uniformly ^{15}N-labeled D1-AB-D2-D3 and D1-D2-D3$^{\Delta AB/linker}$ constructs and recorded their ^{1}H-^{15}N-HSQC spectra. Analysis of the ^{1}H-^{15}N-HSQC spectra of ^{15}N-labeled D1-AB-D2-D3 and D1-D2-D3$^{\Delta AB/linker}$, however, showed that neither of the two ectodomain constructs is tractable by NMR (Figures S2B and S2C). First, out of 340 expected backbone amide peaks for the D1-AB-D2-D3 construct, only ~290 were observed. Similarly, only ~180 out of 318 expected peaks were observed for the D1-D2-D3$^{\Delta AB/linker}$ construct. Second, line shape and intensity of the observed peaks were nonuniform, and a large number of peaks were clustered between 7.6 and 8.6 ppm, a region referred to as random coil region in NMR spectroscopy (Figures S2B and S2C). Since approximately two-thirds of the expected backbone amide proton peaks for each construct were resolved, we suspected that one of the three Ig domains was responsible

2CKN; Kiselyov et al., 2006a). The residues comprising the primary ligand-binding site as experimentally determined by the FGF1-FGFR3c structure, and the secondary ligand-binding site as predicted based on the 2:2:2 FGF2-FGFR1c-heparin complex structure (PDB 1D IFQ9; Schlessinger et al., 2000), are highlighted by red and green boxes, respectively. Residues located at the receptor:receptor interface and the HBS of FGFR3c, as predicted based on the crystal structure of the 2:2:2 FGF2-FGFR1c-heparin complex, are highlighted by gray and dark blue boxes, respectively. See also Figure S1 and Table S1.

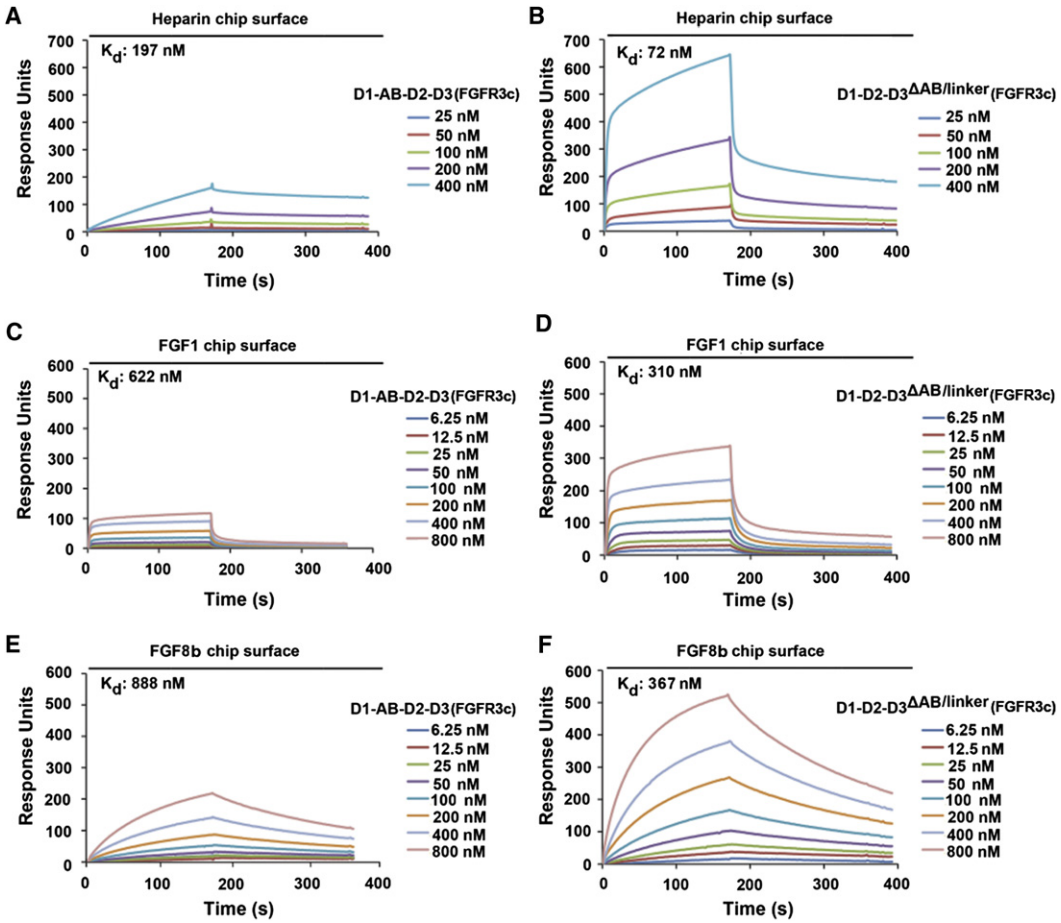

Figure 2. The AB-mediated Autoinhibition of HS- and Ligand-Binding to FGFR3c Is Intrinsically Present in the Context of the Isolated FGFR3c Ectodomain

(A and B) Representative SPR sensorgrams, illustrating binding of (A) the D1-AB-D2-D3 and (B) D1-D2-D3$^{\Delta AB/linker}$ FGFR3c isoforms to heparin. Biotinylated heparin was immobilized on a streptavidin-coated biosensor chip, and increasing concentrations of the receptor ectodomains were passed over the chip.

(C and D) Representative SPR sensorgrams showing binding of (C) D1-AB-D2-D3, and (D) D1-D2-D3$^{\Delta AB/linker}$ to FGF1.

(E and F) Representative SPR sensorgrams illustrating binding of (E) D1-AB-D2-D3 and (F) D1-D2-D3$^{\Delta AB/linker}$ to FGF8b. FGF1 and FGF8b were immobilized via random amine coupling onto a CM5 biosensor chip, and increasing concentrations of the ectodomains were flowed over the chip. See also Figure S2.

for the undesirable behavior of D1-AB-D2-D3 and D1-D2-D3$^{\Delta AB/linker}$ in the HSQC spectra.

To identify this ''problematic'' Ig domain, we generated the following domains/segments of FGFR3c: D1, D1-AB-D2, D1-D2$^{\Delta AB/linker}$, D1-AB/linker, D2, D3, and D2-D3 (Figure S2A; Table S1). The ^{1}H-^{15}N-HSQC spectra of all the receptor fragments lacking D3 exhibited well-dispersed peaks having uniform line width and intensities (Figures S2D–S2H). In contrast, the HSQC spectra of the isolated D3 (Figure S2I) or the D2-D3 fragment (Figure S2J) exhibited a cluster of peaks in the random coil region, reminiscent of the HSQC spectrum of the D1-AB-D2-D3 construct (compare Figures S2I and S2J with Figure S2B). These data, therefore, flagged D3 as the cause of ''bad'' behavior of the D1-AB-D2-D3 and D1-D2-D3$^{\Delta AB/linker}$ constructs in HSQC analysis.

AB-Mediated Autoinhibition of HS Binding Is Intact in the D1-AB-D2 Fragment of FGFR3c

Based on the HSQC profiles, the D1-AB-D2 construct is the longest well-behaved FGFR3 region tractable for structural characterization by NMR. However, the D1-AB-D2 construct cannot be used for investigation of the AB/linker-imposed autoinhibition of ligand binding because X-ray crystal structures of several FGF-FGFR complexes solved by others and us have clearly shown that both D2 and D3 of FGFR are required for ligand binding (Olsen et al., 2006; Plotnikov et al., 1999, 2000; Stauber et al., 2000; Yeh et al., 2003). Since binding of FGFR to HS/heparin is only mediated by D2 (Figures 1A and 1B; Mohammadi et al., 2005a; Schlessinger et al., 2000), we tested whether the AB/linker-mediated autoinhibition of HS binding to D2 still takes place in the context of the D1-AB-D2 construct by comparing the heparin/HS-binding affinity of D1-AB-D2 and D1-D2$^{\Delta AB/linker}$ using SPR spectroscopy. D1-AB-D2 exhibited almost 3-fold lower affinity for heparin than D1-D2$^{\Delta AB/linker}$ (Table 1; Figures S3A and S3B). Importantly, the D1-AB-D2 and D1-AB-D2-D3 constructs experienced a similar degree of loss in HS-binding affinity relative to their AB/linker-lacking counterparts, indicating that AB/linker-mediated autoinhibition of HS binding to receptor is fully intact in the D1-AB-D2 construct

Table 1. Dissociation Constants (Kds) Obtained From SPR Analysis

Receptor Ectodomain Fragment	Heparin	FGF1	FGF8
D1-AB-D2 (FGFR3c)	162	Not studied	Not studied
D1-D2$^{\Delta AB/linker}$ (FGFR3c)	61	Not studied	Not Studied
D1-AB11ALA-D2 (FGFR3c)	53	Not studied	Not studied
D1-AB-D2-D3 (FGFR3c)	197	622	888
D1-D2-D3$^{\Delta AB/linker}$ (FGFR3c)	72	310	367
D1-AB11ALA-D2-D3 (FGFR3c)	78	344	440
AB-D2-D3 (FGFR1c)	207	1230	Not measurable
D1-AB-D2-D3 (FGFR1c)	196	2000	Not measurable
D1-D2-D3$^{\Delta AB}$ (FGFR1c)	68	265	390
D1-AB13ALA-D2-D3 (FGFR1c)	66	268	329

All K_d values are in nanomolar (nM). See also Figures S3 and S4.

(Table 1; Figures 2A and 2B; Figures S3A and S3B). Therefore, we concluded that the D1-AB-D2 construct is suitable for structural characterization of the role of the AB/linker in FGFR autoinhibition.

AB Engages in *cis* the HBS on D2 of FGFR3c

To elucidate the mechanism by which the AB/linker suppresses HS-binding affinity of the D2 region, the backbone resonances of both D1-AB-D2 and D1-D2$^{\Delta AB/linker}$ constructs were assigned. The ^{1}H-^{15}N HSQC spectra of D1-AB-D2 and D1-D2$^{\Delta AB/linker}$ were overlaid, and residues in the D1 and D2 domains that undergo chemical shift changes due to deletion (alternative splicing) of the AB/linker region were identified using a chemical shift difference cutoff of 0.08 ppm (Figure 3A). In D1, the backbone resonances of A36, Q48, L49, V50, F51, G52, S53, E58, S100, D103, and G105 were perturbed (Figure 3B-I; see also Figure 1D for primary sequence) indicating that these D1 residues make intramolecular contacts with D2, AB/linker, or both in the D1-AB-D2 construct. Since neither a crystal nor solution structure of FGFR3c D1 is currently available, these chemically perturbed D1 residues were mapped onto the solution structure of the homologous D1 region of FGFR1c (Kiselyov et al., 2006a; Figure 3C).

The 21 D2 residues that experienced chemical shift perturbations upon deletion (alternative splicing) of the AB/linker region included: T154, R155, E157, R158, M159, D160, K161, K162, L163, N170, V172, R173, F174, C176, A179, G180, N181, W188, F234, Q239, and T240 (Figure 3B-I). In Figure 3D, these D2 residues were mapped onto the molecular surface of the D2 domain taken from the crystal structure of FGF1 complexed with the D2-D3 region of FGFR3c, previously solved in our laboratory (PDB ID 1RY7; Olsen et al., 2004). These NMR data unambiguously show that D2 interacts in *cis* with D1 and/or the AB/linker. Notably, five of the perturbed D2 residues, namely, R155, R158, K161, R173, and R175, belong to the HBS of the receptor (Figures 1B–1D). The observed chemical shift changes of HBS residues in D2, together with the SPR data showing that D1-AB-D2 exhibits lower HS-binding affinity than D1-D2$^{\Delta AB}$, strongly suggest that D1, the AB/linker, or both regions engage in *cis* the HBS of D2 to suppress HS-binding affinity of the D1-AB-D2 construct.

To determine whether D1, AB/linker, or both regions engage the HBS on D2, we assigned backbone resonances of the D1-AB/linker construct and compared them with the corresponding resonances of the D1-AB/linker region from the D1-AB-D2 construct. Deletion of D2 led to perturbation of 11 residues in the D1-AB/linker region, including E37, C119, E135, D136, G137, E138, D139, E140, A141, E142, and D143 (Figure 3B-II). Notably, nine out of eleven perturbed residues, namely, E135, D136, G137, E138, D139, E140, A141, E142, and D143, belong to the AB subregion of the AB/linker (Figure 1D), whereas only two residues from the D1 domain, namely, E37 and C119, are affected. These data, therefore, demonstrate that the negatively charged residues of the AB subregion of the AB/linker electrostatically engage the positively charged HBS on D2 in *cis*, whereas D1 makes only minor contacts with D2.

To fully nail down that the AB subregion is the primary region of the AB/linker that binds D2 intramolecularly, we made a mutated version of D1-AB-D2, in which the eleven primarily acidic residues (residues D133 to D143) of the AB subregion (Figure 1D) were collectively mutated to alanines (D1-AB11ALA-D2; Figure 3E; Table S1). Backbone resonances of the D1 and D2 domains of this construct were assigned and compared with those of the native D1-AB-D2 construct (Figure 3B-III). This chemical shift difference analysis shows that substitution of the AB residues for alanines induces chemical shift perturbations of the very same D2 residues, including the HBS residues, which are perturbed when the AB/linker region altogether is deleted. This conclusion is further corroborated when one compares the chemical shift changes in the D2 region between D1-AB11ALA-D2, D1-D2$^{\Delta AB/linker}$, and the isolated D2 (Figures 3B-IV and 3B-V). This comparison shows essentially no chemical shift differences between these three constructs at the D2 region, confirming that the AB subregion is the primary region of the AB/linker that engages the HBS region of D2 to suppress HS-binding affinity of FGFR.

In order to show that the AB/linker competes with binding of HS to the HBS on D2, increasing concentrations of unlabeled sucrose octasulfate (SOS) were titrated into ^{15}N-labeled D1-AB-D2, and ^{1}H-^{15}N-HSQC spectra of D1-AB-D2 were recorded. Because of difficulties in obtaining homogeneous HS samples, SOS is often used as an analog in structural characterization of FGF and FGFR interactions with HS. Analysis of the HSQC spectra showed that the addition of SOS to D1-AB-D2 results in perturbations of residues in the HBS of D2 (R158, K161, R173, and R175) and in the AB/linker (E135, D136, G137, E142, D143, V146, D147, and T148; Figure 3B-VI). These data demonstrate that the addition of SOS dissociates the intramolecular autoinhibitory contacts between the AB/linker and the HBS on D2. Taken together, these systematic chemical shift difference analyses show that the AB subregion is the principal region of the AB/linker that engages the HBS on D2 to suppress the ability of FGFR to bind to HS. Consistent with this conclusion, D1-AB11ALA-D2 and D1-D2$^{\Delta AB/linker}$ bind heparin with about 3-fold greater affinity than D1-AB-D2 (Table 1; Figures S3A, S3B, and S4A).

To extend our findings to the full-length FGFR3c ectodomain, we made the D1-AB11ALA-D2-D3 construct (Figure 3E;

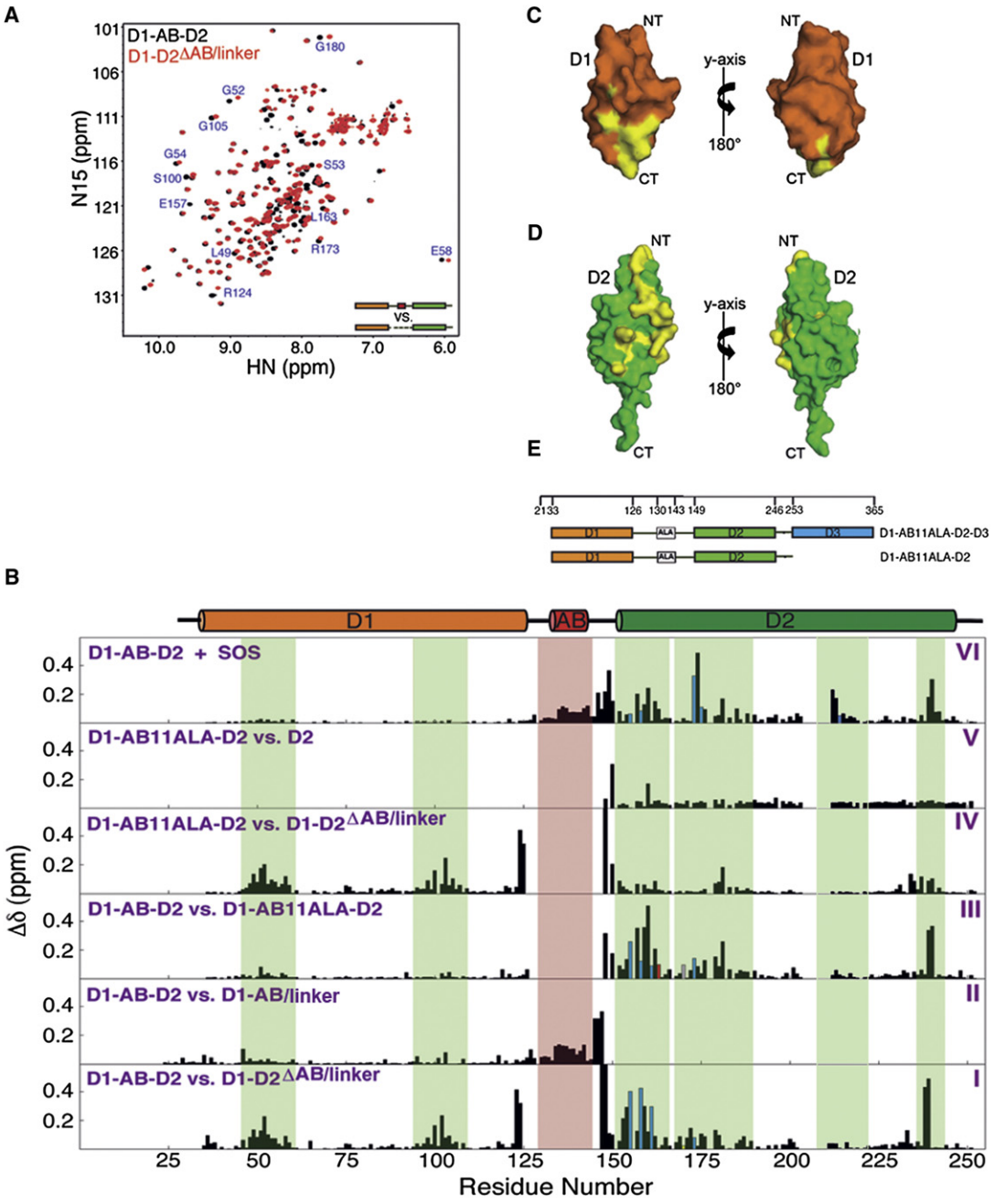

Figure 3. The AB/Linker Region Interacts Intramolecularly with the HBS of D2 in the D1-AB-D2 Fragment of FGFR3c

(A) Overlaid ^{1}H-^{15}N-HSQC spectra of D1-AB-D2 (in black) and D1-D2$^{\Delta AB/linker}$ (in red) isoforms. Some of the residues experiencing significant chemical shift changes are labeled.

The histograms in panel (B) show backbone amide chemical shift differences (Δδ) between (I) D1-AB-D2 and D1-D2$^{\Delta AB/linker}$; (II) D1-AB-D2 and D1-AB/linker; (III) D1-AB-D2 and D1-AB11ALA-D2; (IV) D1-AB11ALA-D2 and D1-D2$^{\Delta AB/linker}$; and (V) D1-AB11ALA-D2 and D2. (VI) The chemical shift differences (Δδ) induced in D1-AB-D2 (100 μM) upon addition of SOS (200 μM). Regions experiencing chemical shift changes greater than 0.08 ppm are highlighted by green and red stripes. Note that residues 204-211, which belong to the secondary ligand-binding site in D2 (Plotnikov et al., 1999), could not be assigned because of their intermediate time scale exchange rate. The significant chemical shift changes observed at the N- and C-terminal regions are expected because of the flexibility of these regions and therefore are not colored. The blue, red, and gray bars denote residues in the D2 domain that participate in HS binding, primary ligand binding, and receptor-receptor interaction, respectively. These perturbed residues are color-coded as in Figure 1D.

(C and D) Residues in D1 and D2, experiencing chemical shift perturbations upon deletion/alternative splicing of the AB/linker from D1-AB-D2, are mapped onto the solution structure of FGFR1 D1 domain (PDB ID 2CKN; Kiselyov et al., 2006a) (C) and D2 domain taken from the crystal structure of FGF1-FGFR3c (PDB ID 1RY7; Olsen et al., 2004) (D). The molecular surfaces of D1 and D2 are colored orange and green, respectively, and the perturbed residues are highlighted in yellow. Note that the deletion of the AB/linker region from D1-AB-D2 induces chemical shift perturbations of D1 residues, whereas selective substitution of the

Table S1) and compared its HS binding affinity to that of D1-AB-D2-D3 and D1-D2-D3$^{\Delta AB/linker}$ using SPR spectroscopy (Figure S4B). D1-AB11ALA-D2-D3 and D1-D2-D3$^{\Delta AB/linker}$ bound HS with similar affinities (K_ds of 78 nM and 72 nM, respectively), which were almost 3-fold greater than that of D1-AB-D2-D3 (Table 1; Figures 2A and 2B; Figure S4B). These data show that as in the D1-AB-D2 construct, the AB subregion interacts with D2 to suppress HS-binding affinity of the full-length FGFR3c ectodomain.

Intramolecular Interaction of the AB Subregion with the HBS of D2 Sterically Suppresses Binding Affinity of FGFR3c for Ligands

Analysis of our chemical shift mapping data show that the *cis* interaction of the AB subregion with the HBS on D2 also perturbs the chemical shift of several D2 residues situated either within (D160) or adjacent to the primary ligand-binding site on D2 (Figure 3B-III). In fact this is anticipated because in the crystal structures of FGF-FGFR complexes the HS-binding site and the primary ligand-binding site on the D2 domain are adjacent to each other (Figure 4A; see also Figure 1D). We inferred from these observations that the interaction of the AB subregion with the HBS on D2 could also sterically interfere with ligand binding to FGFR. To explore this possibility, ligand-binding affinity of the D1-AB11ALA-D2-D3 construct was compared to that of D1-AB-D2-D3 and D1-D2-D3$^{\Delta AB/linker}$ using SPR spectroscopy. The D1-AB11ALA-D2-D3 and D1-D2-D3$^{\Delta AB/linker}$ constructs bound FGF1 and FGF8b with ~2-fold greater affinities than did D1-AB-D2-D3 (Table 1; Figures 2C–2F, 4B, and 4C). These data indicate that the *cis* AB:HBS interaction sterically autoinhibits ligand binding to the receptor, providing a second level of autoinhibition.

D1 Is Dispensable for Autoinhibition of HS Binding to FGFR1c but Plays a Minor Role in Autoinhibition of Ligand Binding to FGFR1c

We next dissected the role of D1 in FGFR autoinhibition. To do so, we decided to make an FGFR3c construct lacking D1 (AB-D2-D3) and compare, by SPR spectroscopy, its HS- and ligand-binding affinities to those of D1-AB-D2-D3. We reasoned that if the AB subregion alone was sufficient for autoinhibition of HS- and ligand-binding to the receptor, then deletion of D1 should have no impact on receptor autoinhibition, that is, the AB-D2-D3 construct should have similar HS- and ligand-binding affinities as the D1-AB-D2-D3 construct. Since the AB-D2-D3 fragment of FGFR3c could not be expressed in *E. coli*, we switched to the analogous construct of FGFR1c (Table S1). As controls, an FGFR1c ectodomain construct lacking the AB subregion of the AB/linker (D1-D2-D3$^{\Delta AB}$) and an FGFR1c construct in which the acidic residues of the AB subregion were replaced by alanines (D1-AB13ALA-D2-D3) were used (Table S1). FGFR1c D1-AB-D2-D3 bound heparin with about 3-fold lower affinity than did both D1-D2-D3$^{\Delta AB}$ and D1-AB13ALA-D2-D3 (Table 1; Figures S5A, S5C, and S5D). Furthermore, the D1-AB-D2-D3 construct bound FGF1 with an approximately 7-fold lower affinity than the D1-D2-D3$^{\Delta AB}$ and D1-AB13ALA-D2-D3 constructs (Table 1; Figures S6A–S6D). The affinity of the D1-AB-D2-D3 construct for FGF8b was too weak to be reliably measured (Figure S6E), whereas the D1-D2-D3$^{\Delta AB}$ and D1-AB13ALA-D2-D3 constructs bound FGF8b with comparable affinity (Table 1; Figures S6G and S6H). These control experiments also convincingly demonstrate that, akin to FGFR3c, the presence of the AB subregion suppresses both HS- and ligand-binding affinity of FGFR1c.

Next, we measured the heparin- and ligand-binding affinities of the AB-D2-D3 construct. As shown in Figure S5, the AB-D2-D3 construct of FGFR1c binds heparin with similar affinity as the D1-AB-D2-D3 construct, indicating that D1 does not play any role in the autoinhibition of HS binding to the receptor (Table 1; Figures S5A and S5B). Only subtle differences in ligand-binding affinity were seen between the AB-D2-D3 and D1-AB-D2-D3 constructs, suggesting that autoinhibition of ligand-binding to the receptor remains nearly intact in the AB-D2-D3 construct. AB-D2-D3 bound FGF1 with slightly greater affinity than did D1-AB-D2-D3 (Table 1; Figures S6A and S6B). The SPR data for FGF8b binding to the D1-AB-D2-D3 and AB-D2-D3 constructs could not be fitted to derive dissociation constants. However, qualitative analysis of the sensorgrams indicates that AB-D2-D3 also binds FGF8b with slightly greater affinity than does D1-AB-D2-D3. This is evidenced by the fact that at any given concentration of either of the two ectodomain constructs, the FGF8b:AB-D2-D3 complex elicits a greater binding response than the FGF8b:D1-AB-D2-D3 complex (compare Figure S6E with Figure S6F). Taken together, these data demonstrate that D1 is dispensable for autoinhibition of HS binding to FGFR but may play a minor role in autoinhibition of ligand binding to FGFR.

The AB Subregion Interacts Transiently with the HBS on D2 of FGFR3c

Collectively, our NMR and SPR data show that the AB subregion interacts in *cis* with the HBS on the D2 domain to directly compete with HS binding and also to sterically inhibit ligand binding to FGFRs. Lastly, we studied the dynamics of the *cis* AB:D2 interaction by collecting heteronuclear NOE data on D1-AB-D2. As shown in Figure 5, the NOE intensities of the AB/linker residues are significantly lower than those belonging to the residues in the well-structured D1 and D2 domains. These data show that the AB/linker is flexible, indicating that the interaction between the AB subregion and the HBS on D2 is of a transient nature.

DISCUSSION

In this report we show that the AB subregion plays a key role in FGFR autoinhibition by engaging in *cis* the HBS of the receptor D2 domain and thereby suppressing HS and FGF binding to the receptor. Because of the close proximity of HS binding and

acidic residues in the AB of the AB/linker region with alanines does not perturb any residues in D1 (compare Figure 3B-I with Figure 3B-II). These observations, therefore, suggest that D1 interacts with the flanking regions of the AB subregion of the AB/linker.
(E) Schematic representation and amino acid boundaries of the alanine-substituted version of FGFR3c constructs generated for chemical shift mapping analyses. D1, D2, D3, and the mutated AB region are colored orange, green, blue, and white, respectively. See Table S1 and Figures S5–S7.

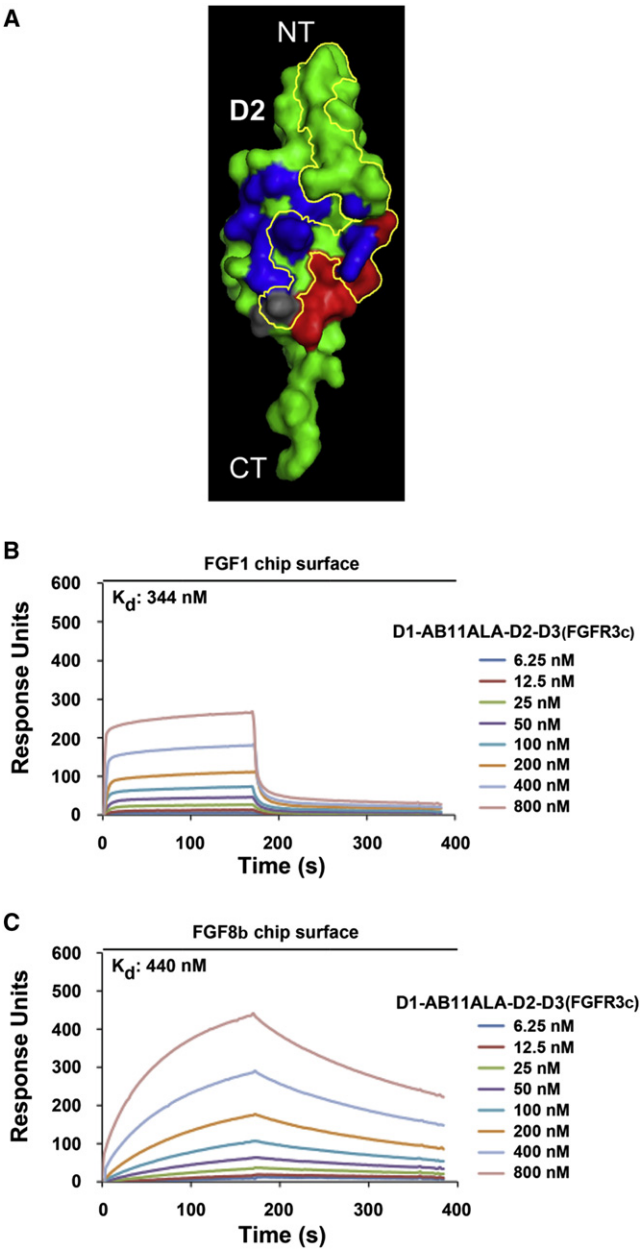

Figure 4. The AB:HBS Interaction Sterically Suppresses Ligand-Binding Affinity of FGFR3c Because of the Close Proximity of Heparin-Binding Site and Primary Ligand-Binding Sites on the D2 Domain

(A) Residues situated in the primary ligand-, the heparin-, and the receptor–receptor binding sites are mapped onto the crystal structure of the D2 domain (PDB ID 1RY7; Olsen et al., 2004). These residues are highlighted in red, blue, and gray, respectively and color-coded are as in Figure 1D. The D2 residues within the yellow boundary are perturbed upon interaction of the AB subregion. (B and C) Representative SPR sensorgrams illustrating binding of D1-AB11ALA-D2-D3 to FGF1 (B) and FGF8b (C). D1-AB11ALA-D2-D3 binds FGF1 and FGF8b with K_ds of 344 nM and 440 nM, respectively. By comparison, D1-AB-D2-D3 binds FGF1 and FGF8b with K_ds of 622 nM and 888 nM, respectively (Figures 2C and 2E). FGF1 and FGF8b were immobilized on a CM5 biosensor chip, and increasing concentrations of the indicated receptor ectodomains were flowed over the chip.

receptor-receptor binding sites on D2, the *cis* AB:HBS interaction also perturbs N170, a key residue that mediates receptor-receptor interaction in the 2:2:2 FGF-FGFR-HS dimer (Figure 3B-III; see also Figure 4A). This finding implies that the intramolecular AB:HBS interaction could also sterically interfere with receptor-receptor binding, perhaps imposing a third level of FGFR autoinhibition, which is autoinhibition of receptor dimerization. These three levels of AB-mediated FGFR autoinhibition act in concert to keep FGF signaling under tight control. In agreement with the key role of the AB subregion in FGFR autoinhibition, sequence analysis of FGFR ectodomains shows that the AB subregion is highly conserved among the four human FGFRs family members and their orthologs (Figures 6A and 6B).

Based on our NMR and SPR data we propose that FGFR exists in an equilibrium between a "closed" and an "open" conformation (Figure 6C). In the closed conformation, the AB subregion engages the HBS of D2 and as a result HS- and ligand-binding affinities of FGFR, and potentially receptor-receptor interaction are suppressed (Figure 6C). Heparan sulfate and FGF preferentially bind to the open conformation, leading to receptor dimerization (Figure 6C). Our NOE data show that the AB transiently interacts with D2 and suggest that the closed and open conformations are equally populated. Thus, FGFR autoinhibition differs from the classic autoinhibition systems, such as the Wiskott-Aldrich syndrome protein (Buck et al., 2004) and the Vav proto-oncoprotein (Li et al., 2008), where over 90% of the molecules are in the autoinhibited state under basal conditions. Our NMR and SPR data, however, suggest that binding of AB to D2 not only suppresses HS binding but also ligand binding and potentially direct receptor-receptor binding necessary for dimerization. Therefore, we believe that although the *cis* AB:D2 interaction is transient, the sum of these three levels of AB-mediated FGFR autoinhibition would provide an effective mechanism to keep FGF signaling under tight control.

As alluded to in the introduction, McKeehan et al. proposed that the AB/linker serves merely as a "passive" tether to facilitate the autoinhibitory intramolecular interactions of D1 with both the HS- and the ligand-binding sites of the D2-D3 regions (Wang et al., 1995). In support of this model, Kiselyov et al. (2006) were able to detect a *trans* interaction between D1 and ligand binding sites on D2 in NMR titration experiments, where 2 mM D1 was titrated into 0.5 mM ^{15}N-labeled D2 and vice versa (Kiselyov et al., 2006b). Our data decisively show that the AB plays an active role in FGFR autoinhibition as opposed to being merely a "passive tether." This is best exemplified by the fact that autoinhibition in FGFR1c and FGFR3c is solely relieved by substituting the acidic residues in the AB subregion with alanines, without changing the length of the AB/linker (Figures S5D and S4B). Furthermore, we do not see any evidence for intramolecular interaction between D1 and the D2-D3 region. Our chemical shift mapping analyses show that the deletion of D2 from the D1-AB-D2 construct induces only minor perturbations in D1 (Figure 3B-II). In addition, overlay of the HSQC spectra of ^{15}N-labeled D1-AB/linker and D1-AB-D2-D3 shows no changes in backbone amide chemical shifts of D1 residues (Figure S7A). Hence, D1 does not interact in *cis* with D2 in either D1-AB-D2 or the intact full-length FGFR3c ectodomains. It is noteworthy that we failed to detect a *trans* interaction between D1 and D2

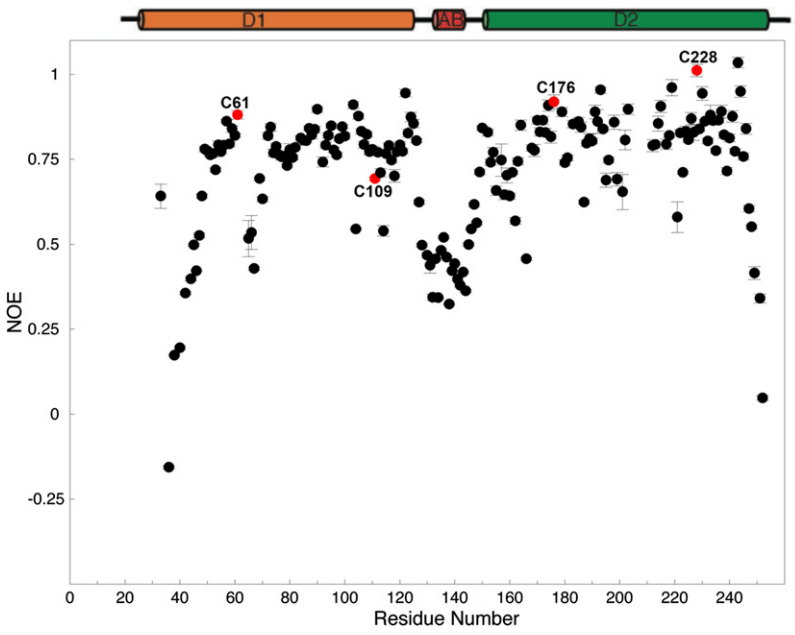

Figure 5. The AB/Linker Region Exhibits Flexibility in the D1-AB-D2 Fragment of FGFR3c

The $^{15}N\{^{1}H\}$NOE is plotted as a function of residue number of the D1-AB-D2 region. Error bars indicate the standard deviation of the NOE intensity determined from three independent measurements. Residues situated in the well-structured D1 and D2 domains exhibit NOE >0.7. In contrast, residues in the AB/linker region show NOE < 0.5, indicating that this region is flexible. As expected, residues of flexible N- and C-termini of the D1-AB-D2 fragment also exhibit NOE <0.5. Individual domain boundaries and the AB/linker region are indicated atop of the plot. NOEs of four cysteines (C61, C109, C176, and C228) that form two disulfide bridges in the well-structured regions of D1 and D2 are labeled and highlighted in red.

in NMR titration experiments using 0.1 mM protein concentrations (Figure S7B). We would surmise that the D1 and D2 domains are connected to each other in the intact ectodomain, so the local concentration of D1 relative to D2 will be much greater than even the concentration at which a *trans* interaction between D1 and D2 was observed (Kiselyov et al., 2006b). Therefore, we should have readily detected a *cis* interaction between D1 and D2 in our D1-AB-D2 and D1-AB-D2-D3 constructs, which are physiologically more relevant systems to study receptor autoinhibition (Figure 3B2; Figure S7A).

Heparan sulfate is abundantly expressed in the pericellular matrix; thus, we speculate that the AB-mediated receptor autoinhibition has evolved to minimize the risk of inadvertent ligand-independent HS-mediated receptor dimerization and activation (Figure 6C). The AB-mediated FGFR autoinhibition may also provide a molecular explanation for the recent finding that the FGFR3c ectodomain inhibits ligand-independent receptor dimerization (Chen et al., 2010). We further suggest that the AB-mediated autoinhibition may also serve as a mechanism to reinforce FGF-binding specificity. Only specific high-affinity ligands that are capable of overcoming the autoinhibition will gain access to the ligand-binding site on the D2-D3 region of receptor. In agreement with this idea, it has been previously shown that the alternatively spliced FGFR3c isoform lacking the AB/linker elicits a strong mitogenic response to FGF2 and FGF4 ligands that are outside the specificity profile of the full-length FGFR3c isoform (Shimizu et al., 2001). The three levels of AB-mediated FGFR autoinhibition along with their effect on FGF-binding specificity would, therefore, provide an elegant mechanism for tight control of FGF signaling in cellular processes, including cell proliferation and differentiation. Loss of this autoinhibitory mechanism underlies several human disorders and malignancies (Onwuazor et al., 2003; Tomlinson and Knowles, 2010), highlighting the importance of this control mechanism in human physiology.

Our model of FGFR ectodomain autoinhibition differs from that of the epidermal growth factor receptor, the only other receptor tyrosine kinase (RTK) for which an autoinhibitory molecular mechanism in the receptor ectodomain has been elucidated to date (Cho and Leahy, 2002; Ferguson et al., 2003). Hence, it appears that different RTKs employ distinct autoinhibitory mechanisms that are probably fine-tuned to their specific physiological functions. Loss of these autoinhibitory mechanisms is a common culprit in human malignancies; therefore, elucidation of these autoinhibitory molecular mechanisms of RTKs should not only shed light onto the molecular etiology of a variety of human diseases but also aid in the discovery of novel drugs for their treatment.

EXPERIMENTAL PROCEDURES

Expression and Purification of FGFR Ectodomain Fragments and FGF Ligands

The details of the receptor and ligand constructs made for this study are given in Table S. A PCR splicing method was used to delete the AB/linker from the D1-AB-D2 and D1-AB-D2-D3 fragments of FGFR3c and the AB subregion from D1-AB-D2-D3 of FGFR1c. Alanine substitutions in the AB subregion of D1-AB-D2-D3 (FGFR3c) and D1-AB-D2 (FGFR3c) were achieved through multiple rounds of site-directed mutagenesis using the Stratagene QuikChange mutagenesis kit. The alanine substitution in the AB subregion of D1-AB-D2-D3 (FGFR1c) was done using a PCR-based mutagenesis method. All constructs were expressed in *E. coli* BL21 (DE3) strain and purified as described in the supplementary material. All proteins were concentrated using Amicon Ultra centrifugal filters (Millipore, Billerica, MA, USA), and protein concentrations were spectrophotometrically determined by measuring absorbance at 280 nm under denaturing conditions using extinction coefficients at 280 nm computed by the ProtParam tool (http://ca.expasy.org/tools/protparam.html). The final concentration of proteins in 25 mM HEPES (pH 7.5) buffer containing 150 mM NaCl buffer fell within the range of 50 μM to 400 μM.

Surface Plasmon Resonance Experiments and Data Processing

SPR experiments were performed at 25°C on a BIAcore 2000 instrument (GE Healthcare, Piscataway, NJ, USA). For heparin binding experiments, biotinylated heparin (Sigma, St. Louis, MO, USA) was noncovalently immobilized on a streptavidin-coated biosensor chip (Sensor Chip SA, GE Healthcare) at a density of approximately 180 RUs in accordance with the manufacturer's instructions. Various purified FGFR1c and FGFR3c ectodomain constructs were then passed over the chip at a flow rate of 50 μl/min at five concentrations (25 nM, 50 nM, 100 nM, 200 nM, and 400 nM). For ligand binding experiments, FGF homologous factor 1b (FHF1b), FGF1, and FGF8b were

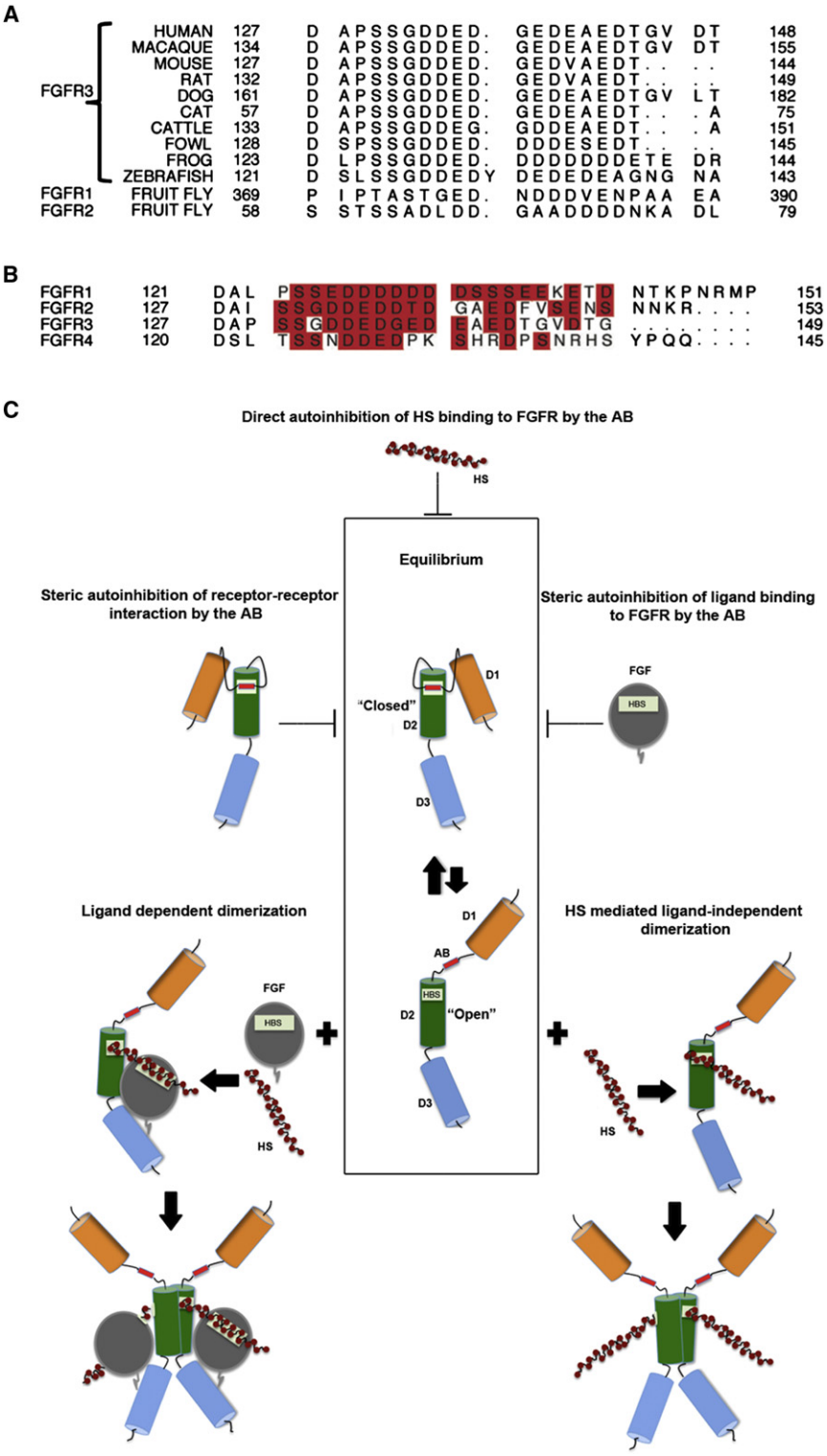

Figure 6. The AB Subregion of the AB/Linker Region Is Highly Conserved among FGFR Orthologs and Acts at Three Levels to Autoinhibit FGFR Signaling

(A) Sequence alignment of the AB/linker region from the indicated FGFR3 orthologs and from fruit fly FGFR1 and FGFR2 indicates that the AB subregion is conserved throughout evolution.

(B) Sequence alignment of the AB/linker region from human FGFR1-FGFR4. The residues highlighted by a red box represent the AB subregion. Periods indicate spaces introduced into the sequences to improve the alignments.

(C) FGFR exists in a dynamic equilibrium between open and closed conformations. In the closed state, the *cis* interaction between the AB subregion and the HBS autoinhibits binding of both HS and ligand to the FGFR, thereby suppressing ligand- and HS-mediated receptor dimerization and subsequent FGFR activation. The *cis* interaction may also sterically inhibit D2-mediated receptor-receptor interaction because of close proximity of the HS and receptor-receptor binding sites on D2. FGF and HS bind to the open state forming the 2:2:2 FGFR:FGF:HS signaling unit. In the open state, the HS binds to the HBS on D2, posing risk of HS-mediated ligand-independent receptor dimerization.

immobilized via random amine coupling on a carboxymethylated dextran biosensor chip (CM5 Sensor chip, GE Healthcare) at a density of about 1300 RUs in accordance with the manufacturer's instructions. Individual FGFR1c and FGFR3c ectodomain constructs were then passed over the chip at a flow rate of 50 μl/min at eight concentrations (6.25 nM, 12.5 nM, 25 nM, 50 nM, 100 nM, 200 nM, 400 nM, and 800 nM). For each concentration, the signal was corrected against the control surface (captured biotin and immobilized FHF1b for the heparin- and ligand-binding experiments, respectively) to eliminate any refractive index changes due to nonspecific binding. Association and dissociation were allowed for 180 s each. The chips were regenerated by HBS-EP buffer (10 mM HEPES-NaOH [pH 7.4], 150 mM NaCl, 3 mM EDTA, 0.005% [v/v] polysorbate 20; GE Healthcare) supplemented with 2 M NaCl. The dissociation constants (K_ds) were calculated by equilibrium steady-state analysis using BiaEvaluation software.

Backbone Assignments of D1-AB-D2, D1-D2$^{\Delta AB/linker}$, D1-AB/linker, D2, and D1-AB11ALA-D2 of FGFR3c

All NMR experiments were performed at 25°C using 600, 700, 800, or 900 MHz Bruker spectrometers equipped with cryoprobes. The concentrations of the isotopically labeled D1-AB-D2 protein, prepared in 25 mM HEPES (pH 7.5) buffer containing 150 mM NaCl and 10% D2O, ranged from 200 μM to 400 μM. The ^{1}H chemical shifts were referenced to water at 4.75 ppm at 25°C, and the ^{13}C and ^{15}N chemical shifts were indirectly referenced using the ^{13}C/^{1}H and ^{15}N/^{1}H ratios, respectively. All of the spectra were processed using nmrPipe, visualized with nmrDraw (Delaglio et al., 1995), and analyzed using NMRView (Johnson, 2004). For the backbone assignment of the ^{2}H, ^{13}C, ^{15}N labeled D1-AB-D2, and D1-D2$^{\Delta AB/linker}$, the following TROSY-based backbone experiments were used: ^{1}H-^{15}N TROSY, trHNCO, trHNCACB, and trHN(CO)CACB. The following NMR spectra were recorded and used for the backbone assignment of D1-AB/linker fragment and D2 segment: ^{1}H-^{15}N HSQC, HNCO, HNCACB, and CBCA(CO)NH. D1-AB11ALA-D2 constructs were assigned by

transferring the backbone assignment from D1-AB/linker, D2, D1-AB-D2, and D1-D2$^{\Delta AB/linker}$.

Chemical Shift Mapping

The following ^{15}N-labeled fragments of FGFR3c were used for the chemical shift mapping analysis: D1-AB/linker, D2, D1-AB-D2, D1-D2$^{\Delta AB/linker}$, D1-AB11ALA-D2, D1-AB-D2-D3, and D1-D2-D3$^{\Delta AB/linker}$. The chemical shift changes ($\Delta\delta$) were calculated using the following Equation (1):

$$\sqrt{(\Delta\delta_{HN})^2 + (0.25 * \Delta\delta_N)^2},$$

where $\Delta\delta_{HN}$ and $\Delta\delta_N$ are the changes in the chemical shifts of ^{1}H and ^{15}N dimensions, respectively, and plotted against the residue number. The cutoff value of 0.08 was chosen based on the average chemical shift difference observed for the entire protein.

Titration Experiments of D1-AB-D2 of FGFR3c with Unlabeled Sucrose Octasulfate

Increasing concentrations of unlabeled SOS (0 μM, 25 μM, 50 μM, 75 μM, 100 μM, 125 μM, 150 μM, 175 μM, and 200 μM) were added continuously as 1 μl increments to a 100 μM solution of ^{15}N-labeled D1-AB-D2 in a 25 mM HEPES (pH 7.5) buffer containing 150 mM NaCl and ^{15}N-HSQC spectra at 25°C were recorded using Bruker spectrometers. The chemical shift differences between the two endpoints were calculated using Equation (1) and plotted against the residue number.

Heteronuclear Overhauser Effect Measurements

The steady state ^{15}N heteronuclear Overhauser effect (NOE) relaxation data sets were recorded by two interleaved spectra, with and without a 4.0 s period of proton saturation, using 48 scans per point (Farrow et al., 1994). The error (σ_{NOE}) was determined using the following Equation (2):

$$\sigma_{NOE} = \frac{I_{sat}}{I_{unsat}}\left[\sqrt{\left(\frac{\sigma_{sat}}{I_{sat}}\right)^2 + \left(\frac{\sigma_{unsat}}{I_{unsat}}\right)^2}\right],$$

where I_{sat} and I_{unsat} represent the measured intensities of a particular resonance in the presence and absence of proton saturation, respectively; σ_{sat} and σ_{unsat} represent the root-mean-square variation in the noise in empty spectral regions of the spectra with and without proton saturation, respectively.

Supplementary Information

Supplemental information includes seven figures, one table, and Supplemental Experimental Procedures and can be found with this article online at doi:10.1016/j.str.2011.10.022.

ACKNOWLEDGMENTS

This work was supported by U.S. National Institutes of Health grants DE13686 (M.M.) and GM47021 (D.C.). Support for the Biacore 2000 SPR instrument was provided by grant P30 NS050276. We are grateful to Dr. Michael Goger for helpful discussions of NMR issues and to Jinghong Ma for preparing the structure figure shown in panel A of Figure 1.

Received: July 11, 2011
Revised: October 18, 2011
Accepted: October 19, 2011
Published: January 10, 2012

REFERENCES

Beenken, A., and Mohammadi, M. (2009). The FGF family: biology, pathophysiology and therapy. Nat. Rev. Drug Discov. *8*, 235–253.

Buck, M., Xu, W., and Rosen, M.K. (2004). A two-state allosteric model for autoinhibition rationalizes WASP signal integration and targeting. J. Mol. Biol. *338*, 271–285.

Chen, H., Xu, C.F., Ma, J., Eliseenkova, A.V., Li, W., Pollock, P.M., Pitteloud, N., Miller, W.T., Neubert, T.A., and Mohammadi, M. (2008). A crystallographic snapshot of tyrosine trans-phosphorylation in action. Proc. Natl. Acad. Sci. USA *105*, 19660–19665.

Chen, L., Placone, J., Novicky, L., and Hristova, K. (2010). The extracellular domain of fibroblast growth factor receptor 3 inhibits ligand-independent dimerization. Sci. Signal. *3*, ra86.

Cho, H.S., and Leahy, D.J. (2002). Structure of the extracellular region of HER3 reveals an interdomain tether. Science *297*, 1330–1333.

Delaglio, F., Grzesiek, S., Vuister, G.W., Zhu, G., Pfeifer, J., and Bax, A. (1995). NMRPipe: a multidimensional spectral processing system based on UNIX pipes. J. Biomol. NMR *6*, 277–293.

Eswarakumar, V.P., Lax, I., and Schlessinger, J. (2005). Cellular signaling by fibroblast growth factor receptors. Cytokine Growth Factor Rev. *16*, 139–149.

Faham, S., Linhardt, R.J., and Rees, D.C. (1998). Diversity does make a difference: fibroblast growth factor-heparin interactions. Curr. Opin. Struct. Biol. *8*, 578–586.

Farrow, N.A., Muhandiram, R., Singer, A.U., Pascal, S.M., Kay, C.M., Gish, G., Shoelson, S.E., Pawson, T., Forman-Kay, J.D., and Kay, L.E. (1994). Backbone dynamics of a free and phosphopeptide-complexed Src homology 2 domain studied by 15N NMR relaxation. Biochemistry *33*, 5984–6003.

Ferguson, K.M., Berger, M.B., Mendrola, J.M., Cho, H.S., Leahy, D.J., and Lemmon, M.A. (2003). EGF activates its receptor by removing interactions that autoinhibit ectodomain dimerization. Mol. Cell *11*, 507–517.

Goetz, R., Beenken, A., Ibrahimi, O.A., Kalinina, J., Olsen, S.K., Eliseenkova, A.V., Xu, C., Neubert, T.A., Zhang, F., Linhardt, R.J., et al. (2007). Molecular insights into the klotho-dependent, endocrine mode of action of fibroblast growth factor 19 subfamily members. Mol. Cell. Biol. *27*, 3417–3428.

Goldfarb, M. (2005). Fibroblast growth factor homologous factors: evolution, structure, and function. Cytokine Growth Factor Rev. *16*, 215–220.

Hou, J., Kan, M., Wang, F., Xu, J.M., Nakahara, M., McBride, G., McKeehan, K., and McKeehan, W.L. (1992). Substitution of putative half-cystine residues in heparin-binding fibroblast growth factor receptors. Loss of binding activity in both two and three loop isoforms. J. Biol. Chem. *267*, 17804–17808.

Itoh, N., and Ornitz, D.M. (2011). Fibroblast growth factors: from molecular evolution to roles in development, metabolism and disease. J. Biochem. *149*, 121–130.

Jin, C., Wang, F., Wu, X., Yu, C., Luo, Y., and McKeehan, W.L. (2004). Directionally specific paracrine communication mediated by epithelial FGF9 to stromal FGFR3 in two-compartment premalignant prostate tumors. Cancer Res. *64*, 4555–4562.

Johnson, B.A. (2004). Using NMRView to visualize and analyze the NMR spectra of macromolecules. Methods Mol. Biol. *278*, 313–352.

Johnson, D.E., and Williams, L.T. (1993). Structural and functional diversity in the FGF receptor multigene family. Adv. Cancer Res. *60*, 1–41.

Kiselyov, V.V., Bock, E., Berezin, V., and Poulsen, F.M. (2006a). NMR structure of the first Ig module of mouse FGFR1. Protein Sci. *15*, 1512–1515.

Kiselyov, V.V., Kochoyan, A., Poulsen, F.M., Bock, E., and Berezin, V. (2006b). Elucidation of the mechanism of the regulatory function of the Ig1 module of the fibroblast growth factor receptor 1. Protein Sci. *15*, 2318–2322.

Kobrin, M.S., Yamanaka, Y., Friess, H., Lopez, M.E., and Korc, M. (1993). Aberrant expression of type I fibroblast growth factor receptor in human pancreatic adenocarcinomas. Cancer Res. *53*, 4741–4744.

Kuro-o, M. (2008). Endocrine FGFs and Klothos: emerging concepts. Trends Endocrinol. Metab. *19*, 239–245.

Li, P., Martins, I.R., Amarasinghe, G.K., and Rosen, M.K. (2008). Internal dynamics control activation and activity of the autoinhibited Vav DH domain. Nat. Struct. Mol. Biol. *15*, 613–618.

Mansson, P.E., Adams, P., Kan, M., and McKeehan, W.L. (1989). Heparin-binding growth factor gene expression and receptor characteristics in normal rat prostate and two transplantable rat prostate tumors. Cancer Res. *49*, 2485–2494.

Mohammadi, M., Dikic, I., Sorokin, A., Burgess, W.H., Jaye, M., and Schlessinger, J. (1996). Identification of six novel autophosphorylation sites

on fibroblast growth factor receptor 1 and elucidation of their importance in receptor activation and signal transduction. Mol. Cell. Biol. *16*, 977–989.

Mohammadi, M., Olsen, S.K., and Goetz, R. (2005a). A protein canyon in the FGF-FGF receptor dimer selects from an à la carte menu of heparan sulfate motifs. Curr. Opin. Struct. Biol. *15*, 506–516.

Mohammadi, M., Olsen, S.K., and Ibrahimi, O.A. (2005b). Structural basis for fibroblast growth factor receptor activation. Cytokine Growth Factor Rev. *16*, 107–137.

Olsen, S.K., Ibrahimi, O.A., Raucci, A., Zhang, F., Eliseenkova, A.V., Yayon, A., Basilico, C., Linhardt, R.J., Schlessinger, J., and Mohammadi, M. (2004). Insights into the molecular basis for fibroblast growth factor receptor autoinhibition and ligand-binding promiscuity. Proc. Natl. Acad. Sci. USA *101*, 935–940.

Olsen, S.K., Li, J.Y., Bromleigh, C., Eliseenkova, A.V., Ibrahimi, O.A., Lao, Z., Zhang, F., Linhardt, R.J., Joyner, A.L., and Mohammadi, M. (2006). Structural basis by which alternative splicing modulates the organizer activity of FGF8 in the brain. Genes Dev. *20*, 185–198.

Onwuazor, O.N., Wen, X.Y., Wang, D.Y., Zhuang, L., Masih-Khan, E., Claudio, J., Barlogie, B., Shaughnessy, J.D., Jr., and Stewart, A.K. (2003). Mutation, SNP, and isoform analysis of fibroblast growth factor receptor 3 (FGFR3) in 150 newly diagnosed multiple myeloma patients. Blood *102*, 772–773.

Orr-Urtreger, A., Bedford, M.T., Burakova, T., Arman, E., Zimmer, Y., Yayon, A., Givol, D., and Lonai, P. (1993). Developmental localization of the splicing alternatives of fibroblast growth factor receptor-2 (FGFR2). Dev. Biol. *158*, 475–486.

Plotnikov, A.N., Schlessinger, J., Hubbard, S.R., and Mohammadi, M. (1999). Structural basis for FGF receptor dimerization and activation. Cell *98*, 641–650.

Plotnikov, A.N., Hubbard, S.R., Schlessinger, J., and Mohammadi, M. (2000). Crystal structures of two FGF-FGFR complexes reveal the determinants of ligand-receptor specificity. Cell *101*, 413–424.

Roghani, M., and Moscatelli, D. (2007). Prostate cells express two isoforms of fibroblast growth factor receptor 1 with different affinities for fibroblast growth factor-2. Prostate *67*, 115–124.

Schlessinger, J., Plotnikov, A.N., Ibrahimi, O.A., Eliseenkova, A.V., Yeh, B.K., Yayon, A., Linhardt, R.J., and Mohammadi, M. (2000). Crystal structure of a ternary FGF-FGFR-heparin complex reveals a dual role for heparin in FGFR binding and dimerization. Mol. Cell *6*, 743–750.

Shi, E., Kan, M., Xu, J., Wang, F., Hou, J., and McKeehan, W.L. (1993). Control of fibroblast growth factor receptor kinase signal transduction by heterodimerization of combinatorial splice variants. Mol. Cell. Biol. *13*, 3907–3918.

Shimizu, A., Tada, K., Shukunami, C., Hiraki, Y., Kurokawa, T., Magane, N., and Kurokawa-Seo, M. (2001). A novel alternatively spliced fibroblast growth factor receptor 3 isoform lacking the acid box domain is expressed during chondrogenic differentiation of ATDC5 cells. J. Biol. Chem. *276*, 11031–11040.

Stauber, D.J., DiGabriele, A.D., and Hendrickson, W.A. (2000). Structural interactions of fibroblast growth factor receptor with its ligands. Proc. Natl. Acad. Sci. USA *97*, 49–54.

Tomlinson, D.C., and Knowles, M.A. (2010). Altered splicing of FGFR1 is associated with high tumor grade and stage and leads to increased sensitivity to FGF1 in bladder cancer. Am. J. Pathol. *177*, 2379–2386.

Wang, F., Kan, M., Yan, G., Xu, J., and McKeehan, W.L. (1995). Alternately spliced NH2-terminal immunoglobulin-like Loop I in the ectodomain of the fibroblast growth factor (FGF) receptor 1 lowers affinity for both heparin and FGF-1. J. Biol. Chem. *270*, 10231–10235.

Xu, J., Nakahara, M., Crabb, J.W., Shi, E., Matuo, Y., Fraser, M., Kan, M., Hou, J., and McKeehan, W.L. (1992). Expression and immunochemical analysis of rat and human fibroblast growth factor receptor (flg) isoforms. J. Biol. Chem. *267*, 17792–17803.

Xu, X., Weinstein, M., Li, C., Naski, M., Cohen, R.I., Ornitz, D.M., Leder, P., and Deng, C. (1998). Fibroblast growth factor receptor 2 (FGFR2)-mediated reciprocal regulation loop between FGF8 and FGF10 is essential for limb induction. Development *125*, 753–765.

Yamaguchi, F., Saya, H., Bruner, J.M., and Morrison, R.S. (1994). Differential expression of two fibroblast growth factor-receptor genes is associated with malignant progression in human astrocytomas. Proc. Natl. Acad. Sci. USA *91*, 484–488.

Yeh, B.K., Igarashi, M., Eliseenkova, A.V., Plotnikov, A.N., Sher, I., Ron, D., Aaronson, S.A., and Mohammadi, M. (2003). Structural basis by which alternative splicing confers specificity in fibroblast growth factor receptors. Proc. Natl. Acad. Sci. USA *100*, 2266–2271.

